Flexible Regulation of Active and Reactive Power for a Fully-controllable V2G Wireless Charger

***Abstract*—Electric Vehicles (EVs) will be an important asset in future power grids, with a dual role as flexible loads and mobile generators. In order to implement a complete set of Vehicle-to-Grid (V2G) services, the EV chargers should be adapted for bidirectional power flow considering both active and reactive power. This paper proposes a simple but effective four-quadrant controller to adjust the two types of power (active and reactive) consumed or generated by the EV. Based on a theoretical analysis, it is developed the formulation to configure the power converts given a command of active and reactive power generated/consumed. As a novelty compared with previous works, any combination of the powers is possible to enable a flexible operation of the V2G wireless charger so that the vehicle can also participate in a wide range of V2G services through a wireless charger. The system is based on the Series-Series (SS) compensation topology, which is one of the most typical structures in wireless chargers. Experimental results at charging power up to 1 kW with a SAE J2954 EV charger prototype demonstrate the validity of the analytical study, in each of the eight operation modes.**

***Index Terms*—active power, bidirectional, electric vehicle, harmonic approximation, magnetic resonant coupling, operation mode, reactive power, V2G control, wireless power transfer.**

NOTATION

Parameters

L_i	Coil self-inductance [H].
C_i	Capacitor value of compensation network [F].
R_i	Coil resistance [Ω].
M	Mutual inductance [H].
n	Order of harmonic.
ω_o	Operating angular frequency [rad/s].
V_{DC}	Primary DC bus voltage [V].
V_{BAT}	Equivalent battery voltage [V].

Variables

i	Subscript adopting the values p for primary and s for secondary circuit.
$v_{i(t)}$	Converter output voltage [V].
$\vec{V_i}$	Converter output voltage, first harmonic approximation [V].
V_i	Converter output voltage, first harmonic approximation, RMS value [V].
$\overline{I_i}$	Current value [A].
P_i	Active power [W].
Q_i	Reactive power [VAr].
P_i^{simp}	Simplified value of active power [W].
Q_i^{simp}	Simplified value of reactive power [VAr].
P^{obj}	Objective active power [W].
Q^{obj}	Objective reactive power [VAr].
δ	Delay between primary and secondary converters [°].
α, β	Phase shift angle for the converter operation [°].

I. INTRODUCTION

The transport sector generates a significant impact on our environment. According to the United States Environmental Protection Agency (EPA), 29% of the nation's greenhouse gas emissions in 2019 were derived from the transportation sector, surpassing the contributions from industry and electricity [1]. These emissions are caused primarily by burning fossil fuels, and could be reduced by developing and adopting sustainable modes of transportation. The EPA foresees Electric Vehicles (EVs) as an opportunity to alleviate this problem. According to the International Energy Agency, the global EV stock is estimated at 140 million with a predicted demand of at least 230 TWh in 2030 [2]. The magnitude of this figure presents both challenges and opportunities for future power systems with a high penetration of renewable energy sources. In this context, EVs can be seen as flexible, controllable loads or mobile generators with a practically null inertia. Vehicle-to-Grid (V2G) refers to the capability of the EV and the charger to revert energy to the grid so that a set of vehicles - controlled by an aggregator - acts as a provider for obligatory and ancillary services such as demand response management, peak power supply, power smoothing and voltage stability [3]. The most common interaction for the bidirectional power flow relates to active power for operational activities such as economic dispatch and frequency regulation [4]. Several works have already analysed that controlled and coordinated consumption/delivery of active power in/from the EVs is effective for the frequency regulation in power systems [5]. In addition, EV chargers can also provide effective services for voltage regulation, for which they perform a compensation by injecting or consuming reactive power [6]. In fact, the EVs could generate/consume reactive power at any State-of-Charge level without impacting life cycle of the batteries. Dealing with the reactive power, the EVs help to regulate the bus voltages in the power system with a fast dynamic and local response [7]. When charging or discharging, EV can inject/withdraw reactive power for the voltage support to the grid [8] . This support can be even provided without any active power consumed by the battery, as stated in [9]. Considering the previous services, it would be suitable to provide the charger with the capability of configuring any combination of active power (P) and reactive power (Q) [10]. The number of modes provided by a control indicates the capability of the EV to participate in the aforementioned grid services.

For these services, the electronics and the controllers of the EV charger must be adapted to allow bidirectional power flow. This adaptation must be performed even for advanced chargers such as EV wireless chargers. For V2G operations, wireless chargers are considered particularly convenient as

they allow the EV charge/discharge to activate autonomously, i.e. without requiring a user to actively participate. Wireless Power Transfer (WPT) includes several technologies, but the most mature of these is based on the induction principle [11]. The basis for this kind of charger is a magnetic field flowing between two air-core coupled coils in the range of 80–90 kHz. Due to this operational frequency, power converters in wireless chargers have a different composition, topology and control when compared with wired chargers. The work in [12] presents a review of the topologies of the power converters in bidirectional wired and wireless chargers. With regard to control, the review in [13] differentiates two main strategies to control the power flow in bidirectional wireless chargers. The difference lies in the way the power converters on the primary and secondary sides are activated. The first strategy consists in activating/deactivating the power converters so that only one acts as an inverter and the other as a rectifier. If the primary converter is configured as an inverter, the power flows from the grid to the battery. Alternatively, when the secondary power converter is controlled as an inverter, the battery delivers power to the grid. In contrast, the second strategy is based on maintaining both power converters as fully controllable, but the activation of both has a delay. In this way, the delay sets the direction of the power flow. This second approach is more complex but results in a more controllable power flow. Grouped according to the previous strategies, Table I extends the analysis done in [13], with a summary of the most relevant and recent contributions on V2G control for EV wireless chargers. They are characterized by the types of power converter they use, their compensation topologies, the goal of the proposed controller and the operation modes they can offer. In this table, 'P' and 'S' stand for the primary and secondary sides respectively. The eight operation modes are illustrated in Fig. 1. Each mode represents a type of combination of P and Q to be delivered or absorbed by the wireless charger. As previously described, the setting of a mode may be linked to the provision of a grid service.

Most V2G proposals for wireless chargers in Table I opt for controlling the flow of active power, that is, they operate at Mode I and II. This is the case of the controller proposed in [14], which is based on the activation and deactivation of the power converters according to the sense of the active power flow. In [15], the same strategy is followed for the control of the power flow but it forces Zero Phase Angle (ZPA) and maximum efficiency. In [16], the authors opt for using the power transfer to code data for the control. A fuzzy logic control is added to adapt the wireless charger to misalignments. The work in [17] also relies on the activation/deactivation of power converters to transfer the power in both senses with asymmetrical input-voltage levels. Based on the delayed activation of the power converters, the works in [18] and [19] also controls the active power flow. The work in [18] proposes a control on the secondary side that does not require any data from the primary side to synchronise the power converters. [20] also focuses on the synchronised power transfer in both senses for active power. The authors in [19] present a novel power stage for the primary side, which is used to transfer the active power flow in both senses with no reactive power. With the described methods, the EVs could not participate in voltage regulation [21]. The work in [22] allows the injection or absorption of reactive power, but its amount is determined by the grid connection and it is non controllable (NC). In fact, no analytical formulation is provided for the setting of reactive power. The proposal in [23] describes a controller which can be set with four different goals. With two of the goals (unity power factor and zero power factor), the controller offers a precise performance of the charger for Modes I, II, III and IV. Any combination of non-null values of P and Q cannot be achieved as the remainder goals of the controller (maximum active power and maximum reactive power) makes the system operate with maximum active or reactive power. Setting one of this type of power to its maximum value already fixes the amount of the other type of power, without any option to adjust its value. The review of the related work shows that there is not a proposed algorithm flexible enough to allow setting any combination of P and Q values. For a fully integration of the EV into the grid services, the power electronics need to be controlled to inject or absorb an accurate amount of active and/or reactive power, that is, to operate in any of the 8 operating modes. The challenge addressed in this paper is how to derive a simple but effective control that enables the participation of the EV in the complete set of the operation modes. This is done with a typical configuration of the power converters and a topology for the compensation systems which is widely used.

It can be observed that most control techniques proposed in the related literature for bidirectional wireless chargers rely on configuring the full-bridges on the primary and secondary sides. Wireless chargers are usually equipped with these converters as they have to tune the system configuration according to the variable conditions on which they may operate, mainly due to coil misalignments [24]. It could be also possible to incorporate a DC/DC converter on the primary side to adjust the power flow as the work in [25] proposed for wired chargers. It basically consists of modulating the voltage of the DC-link. This technique would incur in additional costs. Moreover, the control complexity would increase for a wireless charger to provide the required performance with misalignment. For a precise control of the reactive power, a controlled rectifier may be also necessary between the grid and this new converter. The proposal in [26] demonstrates the increment of the control complexity with the inclusion of the DC-DC converter on the primary side as it requires the adjustment of the three power converters, instead of the two that are controlled with the common topology of the power converters. Consequently, our controller is designed for a full-bridge/full-bridge configuration. Regarding the compensation topology, Series-Series (SS) is the predominant in the related work. There are also some proposals for LCC-LCC and LCL-LCL.

The main contributions of this paper are:

- It presents the design and implementation of a V2G wireless charger with a typical configuration of two full-bridges and a Series-Series compensation topology. The topologies of the power converters are common in EV wireless charger so the proposed controller can be

TABLE I
SUMMARY OF THE MOST RELEVANT CONTRIBUTIONS ON V2G CONTROL FOR EV WIRELESS CHARGERS.

Category	Ref.	Power Converters	Compensation topology	Controller Goal	M1	M2	M3	M4	M5	M6	M7	M8
Activation / Deactivation	[14]	P:Half-bridge (two-switch leg) S:Half-bridge (two-switch leg)	P: C-LC S: LC	Sense of the active power flow	✓	✓						
	[27]	P:Full-bridge S:Full-bridge	P:Series S:Series	Sense of the active power flow with ZPA and maximum efficiency	✓	✓						
	[16]	P:Full-bridge S:Full-bridge	P:Series S:Series	MPPT control	✓	✓						
	[17]	P:Full-bridge S:Full-bridge	P:LCC S:LCC	Sense of the active power flow	✓	✓						
Delay	[28]	P:Full-bridge S:Full-bridge	P:LCL S:LCL	Sense of the power flow with: (i) Maximum active power (ii) Unity power factor (iii) Maximum reactive power (iv) Zero power factor	✓	✓	✓	✓	NC	NC	NC	NC
	[18]	P:Full-bridge S:Full-bridge	P:LCL S:LCL	Regulate the amount and sense of the active power on the secondary side without communication with the primary side.	✓	✓						
	[19]	P:Single stage AC/AC S:Full-bridge	P:Series S:Series	Sense of the power flow with unity PF	✓	✓						
	[22]	P: Full bridge with PFC S: Full-bridge	P: Series S: Series	Sense of the power flow with unity PF and ZVS	✓	✓	NC	NC	NC	NC	NC	NC
	[29]	P:Full-bridge S:Full-bridge	P:LCC S:LCC	Sense of the power flow with unity power factor	✓	✓						
	Proposal	**P:Full-bridge S:Full-bridge**	**P:Series S:Series**	**Any combination of P and Q in both senses of the power flow**	✓	✓	✓	✓	✓	✓	✓	✓

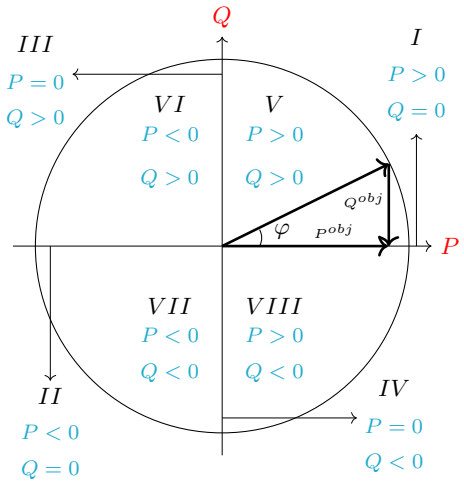

Fig. 1. Operating modes for all four quadrants for a bidirectional wireless charger.

easily adapted for a wide set of systems. As for the compensation network, there is a wide set of EV wireless charger designs with multi-resonant structures but there is also a relevant number of recent proposals with the Series-Series topology. SS is widely used in EV wireless chargers as it can easily cope with coil misalignment and offers high efficiency for the power levels typically managed in these applications [30]. Complementary control techniques (e.g. coil positioning [31] or estimation of the mutual inductance [32]) are considered more advanced and robust when they are based on a Series-Series compensation topology [27].

- The controller functions by delaying the activation of the power converters on the primary and secondary sides. Based on an analytical study, we derive the equations to configure a controller that can effectively work in any position of the four-quadrant diagram with any relation between the active and reactive powers (P^{obj} and Q^{obj} respectively). With this control, the EV gains flexibility to participate in diverse ancillary grid services not only for frequency control - as most of the previous works - but for voltage regulation. As shown in Table I some previous works are restricted to work in some specific conditions (e.g. maximum active power transfer, unity power factor) so they do not contemplate any combination of P and Q , that is, they cannot participate in all the potential services provided for EV conductive chargers.
- The control has been implemented with a synchronisation algorithm and tested for the eight operation modes. From the results, it is concluded that the efficiency is not equivalent for similar power demands with opposite sense of the power flows. Previous works included results for some operation modes (mainly Mode I and II) only as they cannot work in the complete P-Q four-quadrants.

The rest of this paper is structured as follows. In Section II, the analytical study to obtain the equations of the powers in the system is described. We also propose and validate a simplified version of these Equations. Using this analysis, the proposed control is developed in Section III. Section IV describes the experimental validation of the control. Finally, Section V concludes the paper.

II. Analytical study

As mentioned previously, the schematics used in this study follow a conventional topology with a full-bridge controllable DC/AC on the primary and secondary sides. The circuit is shown in Fig. 2. V_{DC} stands for the voltage derived from a primary rectifier and a DC link. V_{BAT} represents the equivalent model of a conventional battery.

The power converters are operated as shown in Fig. 2. It is assumed that the power flow control is based on a phase-delay [13] so that δ corresponds to the time shift of the two converters. Both power converters also execute phase-shifting techniques to control the amount of power flowing in the system by generating a three-level voltage at their output.

In order to obtain the equations of the charger in Fig. 2, it is necessary to know the output voltage of the converters (defined as signals $v_p(t)$ and $v_s(t)$). They correspond to the three-level output of the full-bridge converters. As performed in [13], it can be derived Equations 1 and 2 with a harmonic analysis. The parameter δ is the phase delay between the output of the primary and secondary converter, α and β are the phase shift angles for the operation of the primary and the secondary converter respectively, n is the order of the harmonic and w_o is the operating frequency.

$$v_p(t) = \left(\frac{4}{\pi}\right) V_{DC} \sum_{n=1,3,\dots}^{\infty} \frac{1}{n} \cos\left(n\omega_o t - \frac{n\alpha}{2}\right) \sin\left(\frac{n\alpha}{2}\right) \quad (1)$$

$$v_s(t) = \left(\frac{4}{\pi}\right) V_{BAT} \sum_{n=1,3,\dots}^{\infty} \frac{1}{n} \cos\left(n\omega_o t - \frac{n\alpha}{2} + n\delta\right) \sin\left(\frac{n\beta}{2}\right) \quad (2)$$

Assuming a first harmonic approximation as performed in [33], we obtain the system of equations defined in 3 and 4.

$$\vec{V_p} = \left(R_p + j\omega_o L_p + \frac{1}{j\omega_o C_p}\right)\vec{I_p} - j\omega_o M\vec{I_s} = Z_p\vec{I_p} - j\omega_o M\vec{I_s} \quad (3)$$

$$\vec{V_s} = j\omega_o M\vec{I_p} - \left(R_s + j\omega_o L_s + \frac{1}{j\omega_o C_s}\right)\vec{I_s} = j\omega_o M\vec{I_p} - Z_s\vec{I_s} \quad (4)$$

where $\vec{V_p} = V_p sin\left(\frac{\alpha}{2}\right) \angle 0$ and $\vec{V_s} = V_s sin\left(\frac{\beta}{2}\right) \angle -\delta$. For this formulation, we use RMS phasors so, $V_p = \frac{2\sqrt{2}}{\pi} V_{DC}$ and $V_s = \frac{2\sqrt{2}}{\pi} V_{BAT}$.

Current $\vec{I_p}$ is obtained from equation 3 and $\vec{I_s}$ is calculated in Equation 4 after substituting the value of $\vec{I_p}$ into Equation 5, which yields to:

$$\vec{I_p} = \frac{\vec{V_p} + j\omega_o M\vec{I_s}}{Z_p} \quad (5)$$

$$\vec{I_s} = \frac{\frac{j\omega_o M\vec{V_p}}{Z_p} - \vec{V_s}}{Z_s + \frac{\omega_o^2 M^2}{Z_p}} = \frac{j\omega_o M\vec{V_p} - \vec{V_s}Z_p}{\omega_o^2 M^2 + Z_p Z_s} \quad (6)$$

where

$$Z_p = \left(R_p + j\omega_o L_p + \frac{1}{j2\pi f_o C_p}\right) \quad (7)$$

$$Z_s = \left(R_s + j\omega_o L_s + \frac{1}{j2\pi f_o C_s}\right) \quad (8)$$

and $\omega_o = 2\pi f_o$.

Using Equation 6 in Equation 5, we obtain the following term:

$$\vec{I_p} = \frac{Z_s\vec{V_p} - j\omega_o M\vec{V_s}}{\omega_o^2 M^2 + Z_p Z_s} \quad (9)$$

In order to derive the power, the previous current are defined in a rectangular coordinate form as in Equations 10 and 11,

$$\overline{I_p} = \frac{R_s V_p sin(\frac{\alpha}{2}) - jM\omega_o V_s sin(\frac{\beta}{2})\left(\cos(\delta) - j\sin(\delta)\right)}{R_p R_s + M^2\omega_o^2} \quad (10)$$

$$\overline{I_s} = \frac{jM\omega_o V_p sin(\frac{\alpha}{2}) - V_s sin(\frac{\beta}{2}) R_p\left(\cos(\delta) - j\sin(\delta)\right)}{R_p R_s + M^2\omega_o^2} \quad (11)$$

assuming that at the working frequency ω_o the system is configured so that $j\omega_o L_p = \frac{1}{j\omega_o C_p}$ and $j\omega_o L_s = \frac{1}{j\omega_o C_s}$. Thus the primary and secondary impedances can be simplified as $Z_p = R_p$ and $Z_s = R_s$.

By knowing the currents, it can be determined the active and reactive powers on the primary and secondary sides. Specifically, on the primary side we can state that $P_p = \Re\left(\vec{V_p}\vec{I_p^*}\right)$ and $Q_p = \Im\left(\vec{V_p}\vec{I_p^*}\right)$. For the secondary side, the powers are $P_s = \Re\left(\vec{V_s}\vec{I_s^*}\right)$ and $Q_s = \Im\left(\vec{V_s}\vec{I_s^*}\right)$. With Equations 10 and 11, we derive that:

$$P_p = V_p \sin\left(\frac{\alpha}{2}\right) \frac{V_p \sin\left(\frac{\alpha}{2}\right) R_s - M\omega_o V_s \sin\left(\frac{\beta}{2}\right)\sin(\delta)}{R_p R_s + M^2\omega_o^2} \quad (12)$$

$$Q_p = V_p \left(\frac{M\omega_o V_s}{R_p R_s + M^2\omega_o^2}\right) \sin\left(\frac{\alpha}{2}\right) \sin\left(\frac{\beta}{2}\right) \cos(\delta) \quad (13)$$

$$P_s = V_s \sin\left(\frac{\beta}{2}\right) \left(\frac{-V_s R_p \sin\left(\frac{\beta}{2}\right) - M\omega_o V_p \sin\left(\frac{\alpha}{2}\right)\sin(\delta)}{R_p R_s + M^2\omega_o^2}\right) \quad (14)$$

$$Q_s = V_s \left(\frac{-M\omega_o V_p}{R_p R_s + M^2\omega_o^2}\right) \sin\left(\frac{\alpha}{2}\right) \sin\left(\frac{\beta}{2}\right) \cos(\delta) \quad (15)$$

According to the previous equations, the charger, as a complete load, consumes an active and reactive power (P_p and Q_p respectively), which may be generated power if their values are negative. The values of these powers depend on δ, α and β in a non-linear way. For our further study, it is assume that α = β. Fig. 3 illustrates for a generic prototype – such as the one in [34] – how the P and Q can be modulated by the δ and α parameters. With δ, we could mainly set the sign of these two powers. By setting α, it could be configured the amount of power.

Due to the nonlinearities of the previous equations, it is necessary to further work with the formulae in order to obtain an effective control that could set δ and α in a straightforward

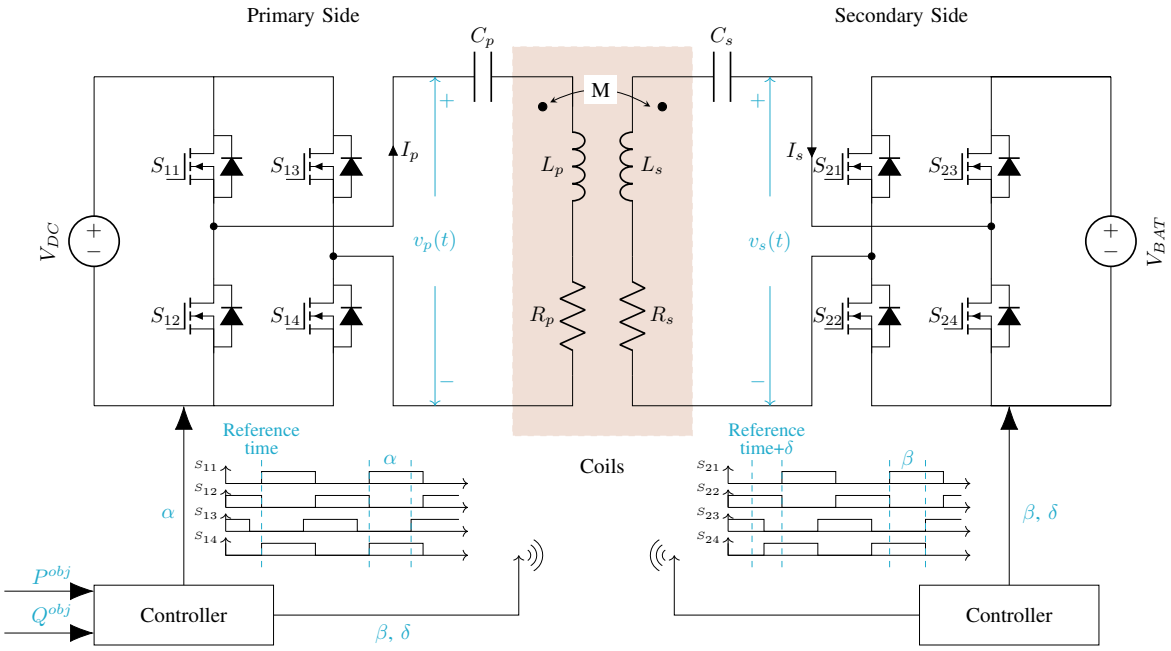

Fig. 2. Complete bidirectional charger circuit with a Series-Series topology.

way. Accordingly, it is assumed that the first term of the numerator in Equation 12 can be reduced so that:

$$V_p sin\left(\frac{\alpha}{2}\right) R_s << M\omega_o V_s \sin\left(\frac{\beta}{2}\right)\sin(\delta) \tag{16}$$

This simplification will be verified in Section IV, once the control is developed. Since the resistances of the power coils are very low, it is also possible to suppress the term R_pR_s in the denominator. If we apply these two simplifications, we obtain a simplified active power on the primary side (P_p^{simp}) in Equation 17.

$$P_p^{simp} = V_p\left(\frac{-V_s}{M\omega_o}\right)\sin\left(\frac{\alpha}{2}\right)\sin\left(\frac{\beta}{2}\right)\sin(\delta) \tag{17}$$

$$P_s^{simp} = V_s\left(\frac{-V_p}{M\omega_o}\right)\sin\left(\frac{\alpha}{2}\right)\sin\left(\frac{\beta}{2}\right)\sin(\delta) \tag{18}$$

As shown in Fig. 4, the simplification involves a minimal variation on this power for 85 kHz. We verified that the simplifications applied previously are indeed valid with different operational frequencies and coupling coefficients, as they both have an effect on the second term of the numerator in Equations 12 and 14. Some controllers vary the operational frequency of the wireless charger to adapt to the varying conditions in which the system may operate [34]. In order to verify the approximation made for different frequencies, we opted to vary this parameter in the range 79 kHz to 90 kHz, which corresponds to the interval set as valid operational frequencies by SAE J2954 [35]. Fig. 4 shows that the variation between the theoretical power and the simplified power is almost imperceptible, especially in the 81 kHz and 84 kHz cases. For the 85 kHz case, a higher value is obtained, but the major difference is observed at 90 kHz, both for P_p and P_s. This slight variation is an offset in the output signal, keeping the amplitude of the peak-to-peak curve constant. For the case of 1 kW, which is the power value reached in our experimental tests, the error is around 1 % with respect to the maximum value of the curve so it can be considered acceptable according to SAE J2954 power levels.

We carried out a similar analysis to check the validity of the simplified equations in misalignment conditions, which may be frequent in EV wireless chargers. We observed an analogous behaviour for the variations of the coupling coefficient, as can be seen in Fig. 5, where k coefficient varies from 0.2 to 0.35. The differences between the simplified power and the initial power are negligible, with a slight deviation observed as the coupling coefficient k decreases. For both tests, the same conclusions are derived for the active power on the secondary side.

III. Proposed Control

Based on the previous analytical study, it is proposed a simple and effective control to set the wireless charger as a consumer or generator of active and reactive power. With an objective of power consumption P^{obj} and Q^{obj}, the system adapts the power converters on the primary and secondary sides to perform accordingly. Specifically, the angles δ, α and β will be calculated to consume the powers set as a goal. Please note that if these variables are set as negative, the system will generate power instead of consuming it.

First, we use Equations 17 and 13, where the tangent of the angle δ can be deduced. In order to simplify the control, we can determine that α = β. In this way,

$$\delta = \arctan\frac{P^{obj}}{Q^{obj}} \tag{19}$$

As there is a division in this computation, it is necessary to carefully set the value of δ so it belongs to the exact quadrant

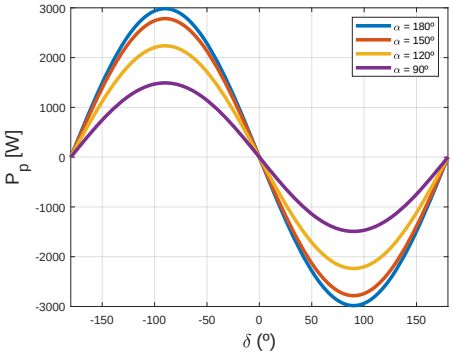

(a) P_p

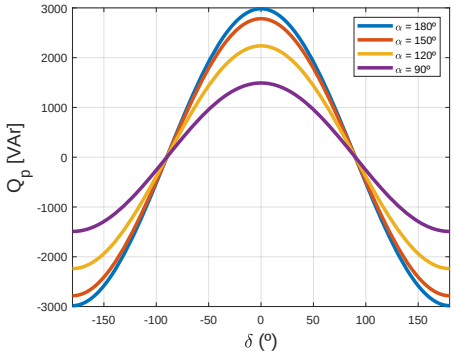

(b) Q_p

Fig. 3. P and Q as a function of α and β.

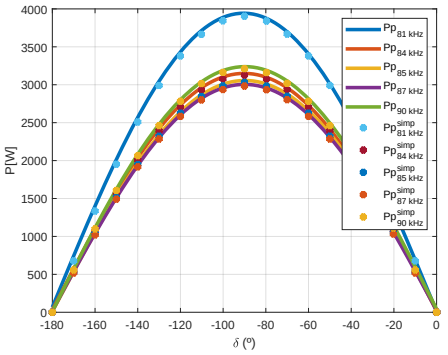

Fig. 4. P_p approximation according to frequency variation.

of Fig. 1. This step is needed because the controller is able to operate in any of the eight modes depicted in the previous Figure. Thus, considering a precision on the setting of the power of 0.001, the ranges for the δ angle can be derived as summarized in Table II. For each mode, we check the simplification formulated in Equation 16, which was required to derive the proposed control. We can conclude that the simplification and, in turn, the control is valid when R_s/M is between 503404 and 503.34. This condition generally holds in

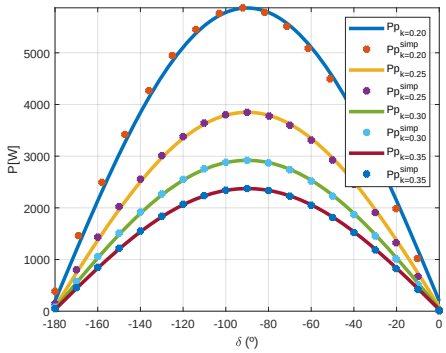

Fig. 5. P_p approximation according to k variation.

EV wireless chargers due to the low values of the resistance of the secondary coil. In fact, the simplification is correct for the prototypes described in the related literature such as those in [27] and [19].

TABLE II
RANGE OF R_s/M ACCORDING TO δ

	δ (º)	$\frac{R_s}{M}$ ($\frac{\Omega}{\mu H}$)
Mode I	270	$\frac{R_s}{M}$ <53407.08
Mode II	90	$\frac{R_s}{M}$ <53407.08
Mode III	180	$\frac{R_s}{M}$ >279.64
Mode IV	0	$\frac{R_s}{M}$ >279.64
Mode V	269.42 < δ <180.54	503.34 < $\frac{R_s}{M}$ <503404.34
Mode VI	179.42 <δ <90.54	540.63 < $\frac{R_s}{M}$ <503404.43
Mode VII	89.42 <δ <0.54	531.30 < $\frac{R_s}{M}$ <503404.43
Mode VIII	-0.54 <δ <-89.42	531.30 < $\frac{R_s}{M}$ <503404.34

For the second part of the control (α calculation), α can be cleared directly by substituting the value of δ in the desired active or reactive power. According to Boucherot's theorem, when the system is configured as $j\omega_o L_p = \frac{1}{j\omega_o C_p}$ and $j\omega_o L_s = \frac{1}{j\omega_o C_s}$, and the coils have a low internal resistance, $P_p \approx P_s$. In this case, we used the secondary power to calculate α, as shown in Equation 20.

$$\alpha = 2 \arcsin\left(\sqrt{\frac{P_s M \omega_o}{-V_p V_s \sin\delta}}\right) \tag{20}$$

As previously commented, the derivation of this control is based on the assumption that Equation 16 is valid. For those values of δ, where this condition does not hold, it is necessary to apply a correction factor.

To implement this algorithm, two controllers should be installed in the wireless charger, as depicted in Fig. 2. Fig. 6 shows the pseudocode of the two controllers. The main controller is installed on the primary side, which receives the commands P^{obj} and Q^{obj} to set. From these inputs, the control algorithm first decides the value for δ with Equation 19. It then checks the quadrant and manipulates the delta value accordingly. Next, it computes α and β according to Equation 20. With the parameter α, the controller on the primary side

Algorithm 1 Control of primary power converter

1. **Input** data: M, L_1, L_2, C_1, C_2, R_2, R_2, ω_o, P^{obj}, Q^{obj}
2. Compute **δ (Eq.18)**
3. Compute **α (Eq.19)**
4. Timer configuration: **α, δ phase shift**
5. **while** (1)
6. Signal generation: **(S11, S13)**
7. **end while**

Algorithm 2 Control and synchronization of secondary power converter

1. **Input** data: M, L_1, L_2, C_1, C_2, R_2, R_2, ω_o, α, δ
2. Reference signal generation
3. Measure initial phase delay
4. Timer configuration: **α, δ phase shift**
5. **while** (1)
6. Phase delay measurement
7. Compute **PI+I** control
8. Compute synchronized **δ**
9. Signal generation: **(S21, S23)**
10. **end while**

Fig. 6. Pseudo-code of algorithms for primary and secondary converters

configures a Pulse Width Modulation (PWM) to adjust the activation signals of the primary converter. This controller also communicates with the controller on the secondary side. With lower computational tasks, this second controller receives the parameters δ and β from the primary controller and sets the corresponding PWM signals for the secondary power converter. A wireless communication is established between the primary and the secondary controllers. The two power converters should be synchronised to have the same time reference for the setting of δ, that is, the phase difference of the output voltage phasors must be maintained at a given constant value equal to δ. For our application, it is necessary to synchronise with a fine resolution as the period of the power signals is 11.76 μs. Estimating the communication latency with a high precision is not trivial as the sequence of communication phases (neighbour discovery, data error, etc.) are not always the same. Moreover, the time for a phase strongly depends on weather conditions or interferences [36]. In the related literature, we can find several electronics solutions for this synchronisation in bidirectional wireless power transfer (BWPT). The work in [37] proposes using an auxiliary coil on the secondary side to detect the phase on the primary circuit. In [38], the authors describe how performing small disturbances on the relative phase helps to set the correct value. An analysis of the power is done for every perturbation and then, small adjustments are performed accordingly. The algorithm explained in [39] bases the synchronisation in a previous circuital analysis and a Phase Locked Loop (PLL). All these methods could be applied in our controller.

If coil misalignment is a possibility, a technique to estimate M is necessary to address Equation 20 correctly. The work in [34] includes the description of a technique to carry out this estimation for a Series-Series WPT as the one used in this paper so it could be easily incorporated for the bidirectional controller. Other parameters as R_p and R_s are constant for the operational frequency range so they can be measured during the manufacturing process and the control could be configured accordingly to these data.

IV. Experimental validation

In order to validate the fully-controllable V2G algorithm, we performed experimental tests on the prototype described in Table III. Fig. 7 shows a photo of the electronics, power sources and the coils used in the laboratory implementation. The coils are made of AWG-38 Litz wire with dimensions according to SAE J2954. They include ferromagnetic materials and shielding on the secondary side.

TABLE III
Characteristics of the analysed wireless charger.

Design frequency (f_o)	85 kHz
Primary coil dimensions	0.51 m × 0.66 m
Resistance of the primary coil (R_p)	85.2 mΩ
Self-inductance of the primary coil (L_p)	60.32 μH
Secondary coil dimensions	0.35 m × 0.35 m
Resistance of the secondary coil (R_s)	118.7 mΩ
Self-inductance of the secondary coil (L_s)	42.08 μH
Mutual inductance (M)	14 μH
Distance between coils assumed in the design (g_d)	0.10 m
Compensation topology	Series-Series
Capacitance of the primary side (C_p)	56.50 nF
Capacitance of the secondary side (C_s)	82.83 nF
Primary DC bus voltage (V_{DC})	150 V
Battery voltage (V_{BAT})	150 V

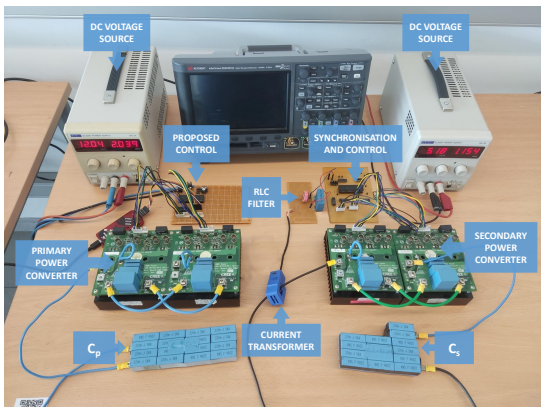

(a) Power electronics.

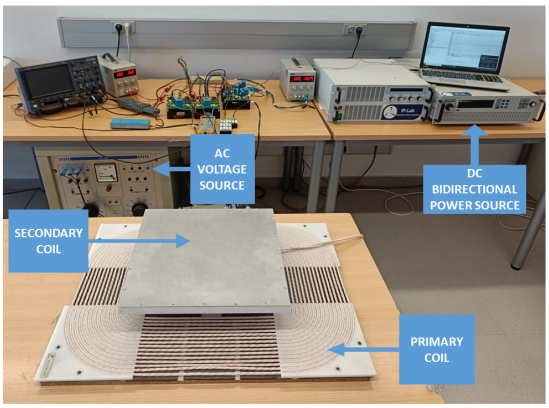

(b) Power sources and coils.

Fig. 7. Power electronics and coils of the prototype.

On primary and secondary sides, we have connected an AC voltage source and a bidirectional power source, model ITECH-BSS2000 to conduct the eight different experiments. They can be seen in Fig. 7.b. The electronics of the power converters and the compensation systems are in Fig. 7.a. In order to conform with the switching frequency and power levels defined in SAE J2954, we developed the full-bridge converter using Silicon Carbide (SiC) MOSFETs. Two CREE evaluation boards KIT8020-CRD-8FF1217P-J make up both legs of the converter. We included two CREE SiC MOSFETS model C2M0080120D, as well as the activation and protection circuitry on each board (e.g. the snubber circuits). These SiC MOSFETs have a low drain-source resistance, which leads to lower switching losses ($R_{ds}^{on} = 80m\Omega$). We also designed the circuit boards so that they reduce switching oscillations and, as a result, electromagnetic interferences (EMI). In order to implement the compensation system, we placed some polypropylene capacitors in series with the main coils. We developed the V2G control system by using a pair of PICKIT4 device, together with two dsPIC30f4011 digital signal processor (DSP) and 74LS04 hex inverters. PICKIT 4 is a programming and debugging development tool which can be used via the graphical user interface of the MPLAB X integrated development environment (IDE).

The operation of both DSPs is synchronised so that the initial target power levels and flow direction are achieved. For the devices synchronisation, a code has been developed based on that described in [39]. First, in one of the DSPs, the final value of δ and α is generated according to the target values of P^{obj} and Q^{obj}. These δ and α values are transmitted wirelessly to the second controller, which must be synchronised. The principle of operation is based on the fact that the secondary current is 90° phase shifted with respect to the primary voltage. Therefore, by measuring this current and shifting the signal through an RLC filter (whose values are $R = 14\ \Omega$, $L_f = 33.85\ \mu H$ and $C_f = 103.73\ nF$, respectively), a signal synchronised with the primary circuit is obtained in the secondary circuit. This signal will be introduced into the secondary control circuit to be used as a reference for the displacement of the δ angle. By means of a PI+I control, the δ angle value is progressively adjusted until the desired final value is reached. The synchronisation time is between 0.2 and 0.3 seconds.

We carried out a set of validation tests for the eight operation modes, being modes V-VIII only possible with our controller and not with other proposals described in the literature. To confirm that we had obtained correct δ and α, we established different objective powers (P^{obj} and Q^{obj}), with one combination for each operating mode. In Table IV experimental δ and α values are shown (δ_{exp} and α_{exp} respectively). We can observe that the experimental values are similar to the values calculated theoretically (δ_{theo} and α_{theo}). They are small differences due to the discretization of the variables and the precision that these micro-controllers have. The screenshot of mode V (Fig. 8) with the four different activation signals (S_{11}, S_{13}, S_{21}, S_{23}) is included as a representative example. In this figure, α, δ and β angles have been highlighted. We can observe that α is related to the activation signals of the primary side and β to the gate signals of the secondary side. In our implementation, we have set that $\alpha = \beta$, which can be visually checked from this figure. The parameter δ refers to the delay between the two pairs of activation signal from different power converters.

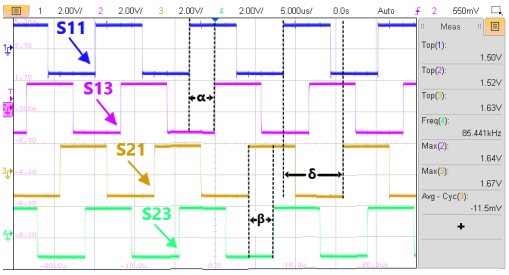

Fig. 8. Activation signals with α, β and δ angles for Mode V.

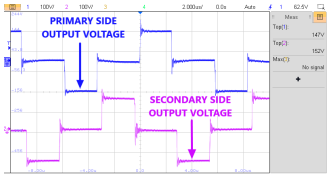

(a) Primary and secondary output voltages.

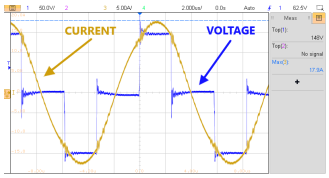

(b) Primary signals.

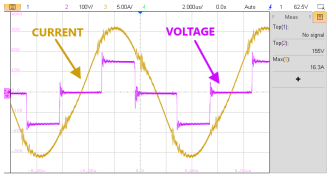

(c) Secondary signals.

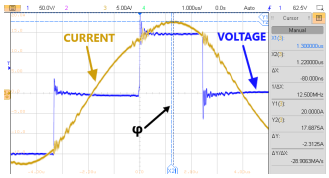

(d) Primary signals zoom.

Fig. 9. Experimental results for Mode I: P_s = 1000 W and Q_s = 0 VAr.

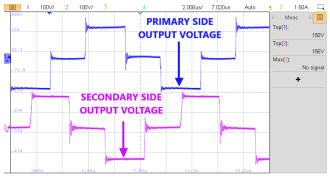

(a) Primary and secondary output voltages.

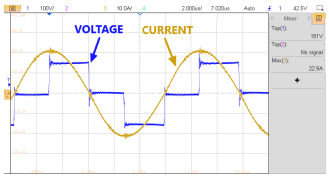

(b) Primary signals.

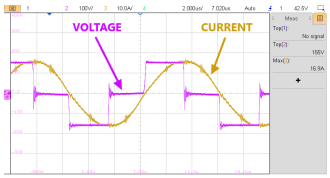

(c) Secondary signals.

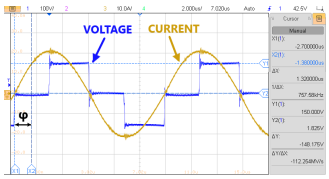

(d) Primary signals zoom.

Fig. 10. Experimental results for Mode V: P_s = 1000 W and Q_s = 1000 VAr.

In Table IV we can observe that the powers obtained (P_p and Q_p) are analogous to the setting (P^{obj} and Q^{obj}) for the eight modes of operation. The minor differences could be due to measurement errors or the nonidealities of the power converters, which were not included in the analytical study.

TABLE IV
PRIMARY CIRCUIT EXPERIMENTAL RESULTS.

Mode	P^{obj}[W]	Q^{obj}[VAr]	$\delta_{theo}[^\circ]$	$\delta_{exp}[^\circ]$	$\alpha_{theo}[^\circ]$	$\alpha_{exp}[^\circ]$	P_p[W]	Q_p[VAr]	η_P[%]	η_Q[%]
I	1000	0	269.99	269.28	67.87	68.21	1040	0	91.023	-
II	-1000	0	90	90.57	67.87	68.21	-954	80	92.42	-
III	0	1000	180	182.17	67.87	68.21	22	1091	-	94.07
IV	0	-750	0	0	57.82	58.32	-23	737	-	90.07
V	1000	1000	225	226.44	83.19	83.89	1065	1063	80.46	81.87
VI	-750	750	135	134.64	70.19	71.56	-751	760	82.40	83.54
VII	-750	-750	45	46.51	70.19	71.56	-764	-756	94.43	93.20
VIII	750	-750	-45	-45.9	70.19	71.56	773	-781	96.17	88.30

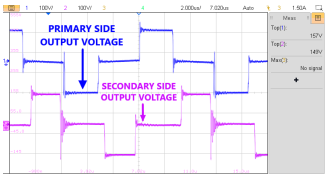

(a) Primary and secondary output voltages.

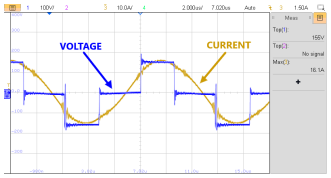

(b) Primary signals.

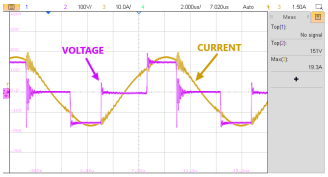

(c) Secondary signals.

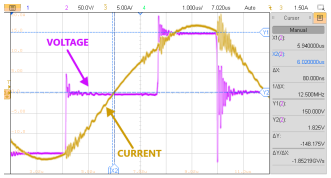

(d) Secondary signals zoom.

Fig. 11. Experimental results for Mode II: P_s = -1000 W and Q_s = 0 VAr.

Thus, the control and the simplifications on which it is based may be considered valid for this system. The efficiency has also been quantified for active and reactive power (η_P and η_Q respectively). The obtained results have been satisfactory, reaching a maximum efficiency value of 96.17 % in mode VIII. This value is within the maximum efficiency values found in the articles in Table I - 96.208 % in [17] -. It should be noted that the system is not symmetric (primary self-inductance is not equivalent to the secondary one), so the charger is not equally efficient in one direction as in the other. For instance, setting the Mode I of the experiments implies a primary current of 17.5 A but in Mode II the current is 16.1 A. This configuration implies that losses due to the coil internal resistances and/or due to non-totally compensated reactive components are different for modes with similar power level but with an opposite sense of the power flow. If we pay attention to the δ parameter, we can conclude that zero voltage switching (ZVS) operation is not guaranteed for all the operation modes. Working at ZVS imposes hard restrictions on the δ angle [40], as it has to be in a range of $-90^\circ < \delta < 90^\circ$. With this restriction, we could not achieve a simple and flexible control with any P and Q as the one that we have developed, so that the possibilities are limited to operation modes VII and VIII.

Three examples of the results can be seen in Fig. 9, where the control was carried out for P_p = 1000 W and Q_p = 0 VAr, in Fig. 10 with P_p = 1000 W and Q_p = 1000 VAr and in Fig. 11 with P_p = -1000 W and Q_p = 0 VAr. We completed Table IV using these and other similar screenshots. We can observe that in Mode I, the first harmonic of the primary voltage and the primary current (Fig. 9.b) are in phase. As there is no reactive power required, the system is operating at resonance. However, for Mode V, this condition does not hold as the system must deliver reactive power (in Fig. 10.b).

V. CONCLUSIONS

Wireless chargers are effective mechanisms for charging EVs, but their performance must be adapted for the future V2G context and services. It is therefore essential to be able to configure them to generate or consume any combination of active power and reactive power. In this paper, we have developed a control algorithm that allows a fully-controllable wireless charger for a common Series-Series topology. The algorithm, which is supported by an analytical study, has been validated by experimental results at charging power up to 1 kW for the complete set of eight operation modes. In contrast to the previous works, the flexible configuration of all the modes, which represent any combination of P and Q, can only be guaranteed with our proposal. Similarly, we have physically incorporated a synchronisation algorithm into our V2G control so that by means of communication between the primary and secondary controller, an exact regulation of the delta angle is achieved in a range of 0.2 to 0.3 seconds. We have demonstrated the validity of both the first harmonic approximation and the mathematical simplification carried out to obtain a simple and effective control.

As future work, we would like to extend the control to search for other configurations of α and β, which may reduce the switching losses.

REFERENCES

[1] "Sources of Greenhouse Gas Emissions — US EPA." [Online]. Available: https://www.epa.gov/ghgemissions/sources-greenhouse-gas-emissions

[2] International Energy Agency (IEA), "Global EV outlook 2019," International Energy Agency (IEA), Tech. Rep., 2019. [Online]. Available: https://www.iea.org/reports/global-ev-outlook-2019

[3] H. M. Khalid, F. Flitti, S. M. Muyeen, M. S. Elmoursi, T. O. Sweidan, and X. Yu, "Parameter estimation of vehicle batteries in V2G systems: An exogenous function-based approach," *IEEE Transactions on Industrial Electronics*, vol. 69, no. 9, pp. 9535–9546, 2022.

[4] B. K. Sovacool, J. Kester, L. Noel, and G. Zarazua de Rubens, "Actors, business models, and innovation activity systems for vehicle-to-grid (V2G) technology: A comprehensive review," p. 109963, 10 2020.

[5] H. Liu, K. Huang, Y. Yang, H. Wei, and S. Ma, "Real-time vehicle-to-grid control for frequency regulation with high frequency regulating signal," *Protection and Control of Modern Power Systems*, vol. 3, 2018. [Online]. Available: https://doi.org/10.1186/s41601-018-0085-1

[6] J. Hu, C. Ye, Y. Ding, J. Tang, and S. Liu, "A distributed MPC to exploit reactive power V2G for real-time voltage regulation in distribution networks," *IEEE Transactions on Smart Grid*, vol. 13, no. 1, pp. 576–588, 9 2021.

[7] S. Islam, A. Iqbal, M. Marzband, I. Khan, and A. M. Al-Wahedi, "State-of-the-art vehicle-to-everything mode of operation of electric vehicles and its future perspectives," *Renewable and Sustainable Energy Reviews*, vol. 166, p. 112574, 2022. [Online]. Available: https://www.sciencedirect.com/science/article/pii/S1364032122004701

[8] J. Wang, G. R. Bharati, S. Paudyal, O. Ceylan, B. P. Bhattarai, and K. S. Myers, "Coordinated electric vehicle charging with reactive power support to distribution grids," *IEEE Transactions on Industrial Informatics*, vol. 15, no. 1, pp. 54–63, 2019.

[9] M. Nikkhah Mojdehi and P. Ghosh, "An on-demand compensation function for an ev as a reactive power service provider," *IEEE Transactions on Vehicular Technology*, vol. 65, no. 6, pp. 4572–4583, 2016.

[10] K. Sevdari, L. Calearo, P. B. Andersen, and M. Marinelli, "Ancillary services and electric vehicles: An overview from charging clusters and chargers technology perspectives," *Renewable and Sustainable Energy Reviews*, vol. 167, p. 112666, 2022. [Online]. Available: https://www.sciencedirect.com/science/article/pii/S1364032122005585

[11] A. Triviño, J. M. González-González, and J. A. Aguado, "Wireless power transfer technologies applied to electric vehicles: A review," *Energies*, vol. 14, no. 6, p. 1547, 3 2021. [Online]. Available: https://doi.org/10.3390/en14061547

[12] A. Sharma and S. Sharma, "Review of power electronics in vehicle-to-grid systems," pp. 337–361, 2 2019.

[13] A. Triviño, J. M. Gonzalez-Gonzalez, and M. Castilla, "Review on control techniques for EV bidirectional wireless chargers," *Electronics 2021, Vol. 10, Page 1905*, vol. 10, no. 16, p. 1905, 8 2021. [Online]. Available: https://www.mdpi.com/2079-9292/10/16/1905/htmhttps://www.mdpi.com/2079-9292/10/16/1905

[14] S. Samanta, A. K. Rathore, and D. J. Thrimawithana, "Bidirectional current-fed half-bridge (C) (LC)-(LC) configuration for inductive wireless power transfer system," *IEEE Transactions on Industry Applications*, vol. 53, no. 4, pp. 4053–4062, 2017.

[15] Y. Liu, U. K. Madawala, R. Mai, and Z. He, "Zero-Phase-Angle controlled bidirectional wireless EV charging systems for large coil misalignments," *IEEE Transactions on Power Electronics*, vol. 35, no. 5, pp. 5343–5353, 2020.

[16] J.-J. Kao, C.-L. Lin, Y.-C. Liu, C.-C. Huang, and H.-S. Jian, "Adaptive bidirectional inductive power and data transmission system," *IEEE Transactions on Power Electronics*, vol. 36, no. 7, pp. 7550–7563, 2021.

[17] M. Mohammad, O. C. Onar, G.-J. Su, J. Pries, V. P. Galigekere, S. Anwar, E. Asa, J. Wilkins, R. Wiles, C. P. White, and L. E. Seiber, "Bidirectional LCC-LCC-compensated 20-kW wireless power transfer system for medium-duty vehicle charging," *IEEE Transactions on Transportation Electrification*, vol. 7, no. 3, pp. 1205–1218, 2021.

[18] Y. Tang, Y. Chen, U. K. Madawala, D. J. Thrimawithana, and H. Ma, "A new controller for bidirectional wireless power transfer systems," *IEEE Transactions on Power Electronics*, vol. 33, no. 10, pp. 9076–9087, 2018.

[19] B. Vardani and N. R. Tummuru, "A single-stage bidirectional inductive power transfer system with closed-loop current control strategy," *IEEE Transactions on Transportation Electrification*, vol. 6, no. 3, pp. 948–957, 2020.

[20] Y. Zhang, Y. Guo, L. Wang, Q. Bo, and Z. Liu, "An optimization method of dual-side lcc compensation networks simultaneously considering output power and transmission efficiency in two directions for bwpt systems," *IEEE Journal of Emerging and Selected Topics in Industrial Electronics*, vol. 3, no. 3, pp. 500–508, 2022.

[21] E. R. Joy, K. Thirugnanam, M. Singh, and P. Kumar, "Distributed active and reactive power transfer for voltage regulation using V2G system," in *2015 4th International Conference on Electric Power and Energy Conversion Systems, EPECS 2015*. Institute of Electrical and Electronics Engineers Inc., 12 2015.

[22] J. Liu, F. Xu, C. Sun, and K. H. Loo, "A soft-switched power-factor-corrected single-phase bidirectional AC-DC wireless power transfer converter with an integrated power stage," *IEEE Transactions on Power Electronics*, vol. 37, no. 8, pp. 10 029–10 044, 2022.

[23] A. A. S. Mohamed, A. Berzoy, F. G. N. de Almeida, and O. Mohammed, "Modeling and assessment analysis of various compensation topologies in bidirectional IWPT system for EV applications," *IEEE Transactions on Industry Applications*, vol. 53, no. 5, pp. 4973–4984, 9 2017. [Online]. Available: http://ieeexplore.ieee.org/document/7917270/

[24] V.-B. Vu, A. Ramezani, A. Triviño, J. M. Gonzalez-Gonzalez, N. B. Kadandani, M. Dahidah, V. Pickert, M. Narimani, and J. Aguado, "Operation of inductive charging systems under misalignment conditions: A review for electric vehicles," *IEEE Transactions on Transportation Electrification*, pp. 1–1, 2022.

[25] S. H. Hosseini, R. Ghazi, and H. Heydari-Doostabad, "An extendable quadratic bidirectional DC-DC converter for V2G and G2V applications," *IEEE Transactions on Industrial Electronics*, vol. 68, no. 6, pp. 4859–4869, 2021.

[26] L. Wang, U. K. Madawala, and M.-C. Wong, "A wireless vehicle-to-grid-to-home power interface with an adaptive DC link," *IEEE Journal of Emerging and Selected Topics in Power Electronics*, vol. 9, no. 2, pp. 2373–2383, 2021.

[27] S. Liu, R. Mai, L. Zhou, Y. Li, J. Hu, Z. He, Z. Yan, and S. Wang, "Dynamic improvement of inductive power transfer systems with maximum energy efficiency tracking using model predictive control: analysis and experimental verification," *IEEE Transactions on Power Electronics*, vol. 35, no. 12, pp. 12 752–12 764, dec 2020.

[28] A. A. S. Mohamed, A. Berzoy, and O. A. Mohammed, "Experimental validation of comprehensive steady-state analytical model of bidirectional wpt system in evs applications," *IEEE Transactions on Vehicular Technology*, vol. 66, no. 7, pp. 5584–5594, 2017.

[29] D. Zhang, M. Chen, B. Li, X. Wang, X. Sun, and F. Jiang, "Synchronization strategy based on resonant current detection for bidirectional wireless charging system," *IEEE Transactions on Power Electronics*, vol. 37, no. 9, pp. 11 436–11 449, 2022.

[30] R. K. Jha, G. Buja, M. Bertoluzzo, S. Giacomuzzi, and K. N. Mude, "Performance comparison of the one-element resonant EV wireless battery chargers," *IEEE Transactions on Industry Applications*, vol. 54, no. 3, pp. 2471–2482, 1 2018.

[31] A. Namadmalan, R. Tavakoli, S. Goetz, and Z. Pantic, "Self-aligning capability of IPT pads for high-power wireless EV charging stations," *IEEE Transactions on Industry Applications*, pp. 1–1, 2022.

[32] J. Zeng, S. Chen, Y. Yang, and S. Y. R. Hui, "A primary-side method for ultra-fast determination of mutual coupling coefficient in milliseconds for wireless power transfer systems," *IEEE Transactions on Power Electronics*, pp. 1–11, 2022.

[33] A. A. S. Mohamed and O. Mohammed, "Bilayer predictive power flow controller for bidirectional operation of wirelessly connected electric vehicles," *IEEE Transactions on Industry Applications*, vol. 55, no. 4, pp. 4258–4267, 2019.

[34] J. M. Gonzalez-Gonzalez, A. Triviño-Cabrera, and J. A. Aguado, "Model predictive control to maximize the efficiency in EV wireless chargers," *IEEE Transactions on Industrial Electronics*, vol. 69, no. 2, pp. 1244–1253, 2022.

[35] SAE International, "SAE J2954B: Wireless Power Transfer for Light-Duty Plug-in/Electric Vehicles and Alignment Methodology," 2019.

[36] J. Tosi, F. Taffoni, M. Santacatterina, R. Sannino, and D. Formica, "Performance evaluation of bluetooth low energy: A systematic review," *Sensors*, vol. 17, no. 12, 2017. [Online]. Available: https://www.mdpi.com/1424-8220/17/12/2898

[37] D. J. Thrimawithana, U. K. Madawala, and M. Neath, "A synchronization technique for bidirectional IPT systems," *IEEE Transactions on Industrial Electronics*, vol. 60, no. 1, pp. 301–309, 2013.

[38] F. Liu, K. Li, K. Chen, and Z. Zhao, "A phase synchronization technique based on perturbation and observation for bidirectional wireless power transfer system," *IEEE Journal of Emerging and Selected Topics in Power Electronics*, vol. 8, no. 2, pp. 1287–1297, 2020.

[39] S. Jia, C. Chen, P. Liu, and S. Duan, "A digital phase synchronization method for bidirectional inductive power transfer," *IEEE Transactions on Industrial Electronics*, vol. 67, no. 8, pp. 6450–6460, 2020.

[40] Y. Jiang, L. Wang, J. Fang, R. Li, R. Han, and Y. Wang, "A high-efficiency ZVS wireless power transfer system for electric vehicle charging with variable angle phase shift control," *IEEE Journal of Emerging and Selected Topics in Power Electronics*, vol. 9, no. 2, pp. 2356–2372, 2021.